A visible edge aware directional total variation model for limited-angle reconstruction

Yinghui Zhang[a], Ke Chen[b], Xing Zhao[a], and Hongwei Li*[a]

[a] School of Mathematical Sciences, Capital Normal University, Beijing, 100048, China
[b]Department of Mathematical Sciences, University of Liverpool, L693BX, United Kingdom.

ABSTRACT

The directional total variation algorithm (DTV) reported in the literature achieves promising results for limited angle reconstructions, especially when the scanning angular range is very small. However, the visible edge prior for limited-angle CT is not explicitly considered by DTV. In this paper, a variant of the DTV model is proposed which explicitly builds into the visible edge prior developed by Quinto et al. Numerical experiments show that the proposed model and algorithm produce very competitive results compared to DTV.

Keywords: limited-angle CT, directional total variation, iteration reconstruction.

1. INTRODUCTION

In certain computed tomography (CT) applications, due to the restrictions on the scanning condition or the geometrical shapes of scanning objects, the projection data could be only acquired in a limited angular range which leads to the challenging limited-angle reconstruction problem. This happens in both medical diagnosis like breast imaging[1] and industrial inspection like the C-arm neuro imaging.[2]

Conventional reconstruction methods like filtered back-projection (FBP) and (simultaneous) algebraic reconstruction technique ((S)ART) perform poorly with limited-angle data, introducing heavy image blurring along the directions perpendicular to the missing projection rays. The limited-angle reconstruction problem has been extensively studied for decades, including theoretical characterization and practical reconstruction algorithms.

An early method views it as a projection domain inpainting problem[3] and incorporate the smoothness prior of projection data into the reconstruction process. However, since a local extrapolation error in the projection domain may cause global artifacts in the image domain, this kind of methods suffers from severe stability issue. Another method is based on optimization models encoded with various hand-crafted priors. In certain applications, CT images can be approximated well by piecewise constant functions which should possess the gradient sparsity property. This property can be encoded by the total variation (TV) regularizer, extensively used in image processing. The first method adopting TV regularization is introduced in[4] for divergent CT reconstruction. Since then, various modifications and improvements have been proposed, including the adaptive steepest descent-projection onto a convex set method,[5] prior image constrained compressed sensing method,[6] adaptive-weighted TV model,[7] TV-l_0 gradient minimization,[?] etc. These methods could effectively improve the reconstruction quality and achieve promising results.

For limited-angle reconstruction, there is a vital prior described by the theory of visible and invisible boundaries[8] developed by Quinto et al. This prior is first considered by the anisotropic total variation (ATV) method.[9] Later on, the reweighted ATV[10] method takes projection directions as prior information and combines them into the TV formulation. Especially, the alternating edge-reserving diffusion and smoothing (AEDS) algorithm[11] takes the visible edges prior to its full advantage. By designing separated x- and y-direction regularizers, the AEDS model encodes explicitly the visible edges prior, and by adopting the alternating minimization technique, the AEDS algorithm decouples the x-direction regularization from the y-direction regularization such that the visible edges are protected and utilized to their full advantages.

Further author information: (Send correspondence to Hongwei Li)
Hongwei Li: E-mail: hongwei.li91@cnu.edu.cn

7th International Conference on Image Formation in X-Ray Computed Tomography,
edited by Joseph Webster Stayman, Proc. of SPIE Vol. 12304, 123042N
© 2022 SPIE · 0277-786X · doi: 10.1117/12.2647520

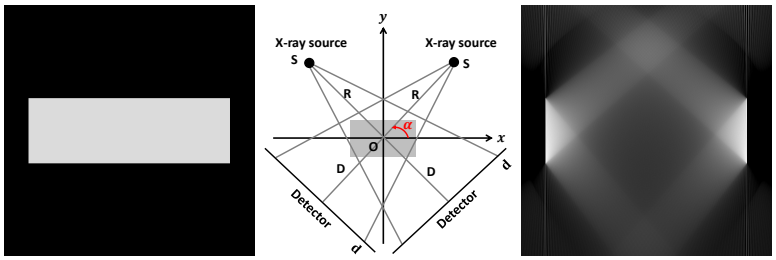

(a) Phantom (b) Configuration (c) FBP

Figure 1: Illustration of the theory of visible and invisible boundaries. (a) The rectangle phantom; (b) the scanning configuration; (c) the limited-angle reconstruction for the scanning angular range ($[\frac{\pi}{4}, \frac{3\pi}{4}]$).

A very recent algorithm named DTV (directional total variation) is proposed in,[12] which shows very promising reconstructions, especially for very small scanning angular ranges. The energy functional associated with DTV can be seen as a reformulation or constrained version of the AEDS model when the regularizers are specified by x-direction TV (TV_x) and y-direction TV (TV_y). The workhorse of DTV is the primal-dual based Chambolle-Pock (CP) algorithm.

Motivated by the success of the DTV algorithm, we propose to reformulate the DTV model such that the new model treats the visible edges prior (corresponding to TV_x) differently from TV_y. This is achieved by exchanging the roles of TV_x and the data fidelity terms. Since the TV_x term goes into the energy functional while the TV_y term is specified as a constraint, the new model shall treat them differently. In this way, we think that the visible edges prior could be better utilized.

The remainder of this paper is organized as follows. We present our approach to the limited-angle CT reconstruction problem in Section 2. In Section 3, experiments are carried out to validate the proposed method. Finally, we conclude the paper in Section 4.

2. METHOD

2.1 The limited-angle CT reconstruction problem

Assume that the size of reconstruction image u is $M \times N$. The vector $\overrightarrow{u} \in \mathbb{R}^J, J = M \times N$ is a concatenate form along the columns of u, and u_i describes the ith entry of $\overrightarrow{u}, i = 1, 2, \ldots, J$. The CT reconstruction problem could be formulated as solving a linear system

$$A\overrightarrow{u} = \overrightarrow{b} + \overrightarrow{\epsilon}, \tag{1}$$

where $A \in \mathbb{R}^{I \times J}$ is the system matrix and $\overrightarrow{b}$ is a vector of length $I = V \times D$ which represents the acquired projection data. V and D denote the number of projection views and the number of detector cells, respectively. $\overrightarrow{\epsilon}$ accounts for any measurement bias and additive noise.

For limited-angle data, the linear system (1) with $I \ll J$ is severely ill-posed, therefore, images reconstructed by conventional reconstruction algorithms will introduce streak and blurring artifacts. This is demonstrated in Fig.(1). Without loss of generality, here, we consider the fan-beam scanning with limited-angle range ($[\frac{\pi}{4}, \frac{3\pi}{4}]$). The rectangle phantom and the scanning configuration are shown in Fig.(1a) and Fig.(1b), respectively. Under this scanning configuration, according to the theory of visible and invisible boundaries, the edges close to vertical are visible and can be easily reconstructed, while for the edges close to be horizontal will be invisible and cannot be recovered well by conventional reconstruction algorithms like FBP or SART, as shown in Fig.(1c).

2.2 The DTV model

The DTV algorithm[12] is to solve the following minimization problem

$$\begin{aligned} &\overrightarrow{u}^\star = \min_u \frac{1}{2}\|A\overrightarrow{u} - \overrightarrow{b}\|_2^2 \\ &s.t.\ \|\nabla_x \overrightarrow{u}\|_1 \le t_x,\ \|\nabla_y \overrightarrow{u}\|_1 \le t_y,\ \overrightarrow{u} \ge 0, \end{aligned} \tag{2}$$

where ∇_x and ∇_y represent matrices size of $J \times J$, corresponding to the discrete x-direction and y-direction gradient operators, respectively, and t_x and t_y are two scalars, specifying the allowed total variations along the x-direction and y-direction, respectively. Since the model (2) is convex, the CP algorithm could be employed to compute a global minimizer. It should be noted that for limited-angle problems, the matrix A has a very large kernel space, so that the model (2) could possess multiple global minimizers. In this case, different parameterizations or different initializations could lead to different solutions.

2.3 The visible edge aware DTV model (VEA-DTV)

As mentioned earlier, to better utilize the visible edges prior, we reformulate the DTV model (2) as the following one

$$\begin{aligned} &\overrightarrow{u}^\star = \min_u \|\nabla_x \overrightarrow{u}\|_1 \\ &s.t. \|A\overrightarrow{u} - \overrightarrow{b}\|_2 \le \epsilon,\ \|\nabla_y \overrightarrow{u}\|_1 \le t_y,\ \overrightarrow{u} \ge 0. \end{aligned} \tag{3}$$

The parameter ϵ controls the noise-level of reconstructed image, which has a clear physical meaning.[13] It's easy to check that

$$\ker(A) \cap (\ker(\nabla_x) \cup \ker(\nabla_y)) = \{0\}, \tag{4}$$

so the proposed VEA-DTV model (3) is theoretically equivalent to the DTV model (2). However, since the two formulations are not the same, when applying the CP algorithm, the resulting solving algorithms would be different. As mentioned earlier, for limited-angle problems, the models (3) and (2) are not strictly convex and since the system matrix A has a large kernel space, each of the two models admits multiple solutions, in which case different algorithms might reach different global minimizers. So, starting from the formulation (3), the CP algorithm might compute a solution different from that of the DTV algorithm. This is also the case when comparing AEDS and DTV. The model AEDS(l_1, l_1) coincides exactly with that of DTV, since condition (4) is met. However, since AEDS and DTV employ different minimization algorithms, their performance could be different. In fact, the alternating minimization algorithm adopted by AEDS takes constant step-sizes, according to the framework of incremental methods,[14] it only converges to a neighbourhood of the optimum. On the other hand, the CP algorithm can be proved to converges to a saddle point corresponding to a optimum.

2.4 Numerical algorithm

The CP algorithm is adapted to develop an iterative algorithm for solving (3) by

$$\begin{aligned} \overrightarrow{u}^\star = \min_u\ & \nu_1 \|\nabla_x \overrightarrow{u}\|_1 + \delta_{\mathrm{Ball}(\epsilon)}(A\overrightarrow{u} - \overrightarrow{b}) \\ & + \delta_{\mathrm{Diamond}(\nu_2 t_y)}(\nu_2 |\nabla_y \overrightarrow{u}|_1) + \delta_{\mathrm{P}}(\mu \overrightarrow{u}), \end{aligned} \tag{5}$$

where indicator functions $\delta_{\mathrm{Ball}}(\overrightarrow{x}), \delta_P(\overrightarrow{x}), \delta_{\mathrm{Diamond}(a)}(\overrightarrow{x})$ are defined as:

$$\delta_{\mathrm{Ball}(\epsilon)}(\overrightarrow{x}) = \begin{cases} 0, & \|\overrightarrow{x}\|_2 \le \epsilon \\ \infty, & \|\overrightarrow{x}\|_2 > \epsilon \end{cases}, \delta_{\mathrm{P}}(\overrightarrow{x}) = \begin{cases} 0, & \overrightarrow{x} \ge 0 \\ \infty, & \overrightarrow{x} < 0 \end{cases},$$

$$\delta_{\mathrm{Diamond}(a)}(\overrightarrow{x}) = \begin{cases} 0, & \|\overrightarrow{x}\|_1 \le a \\ \infty, & \|\overrightarrow{x}\|_1 > a \end{cases}.$$

Then, the min-max formulation of (5) is given by

$$\begin{aligned} &\left(\overrightarrow{u}^\star, \overrightarrow{w}^\star, \overrightarrow{p}^\star, \overrightarrow{q}^\star, \overrightarrow{t}^\star\right) = \min_{\overrightarrow{u}} \max_{\overrightarrow{w},\overrightarrow{p},\overrightarrow{q},\overrightarrow{t}} \langle \nu_1 \nabla_x \overrightarrow{u}, \overrightarrow{p}\rangle \\ &- \delta_{\mathrm{Box}(1)}(|\overrightarrow{p}|) + \langle A\overrightarrow{u} - \overrightarrow{b}, \overrightarrow{w}\rangle - \epsilon\|\overrightarrow{w}\|_2 + \langle \nu_2 \nabla_y \overrightarrow{u}, \overrightarrow{q}\rangle \\ &- \nu_2 t_y \|(|\overrightarrow{q}|)\|_\infty + \langle \mu\overrightarrow{u}, \overrightarrow{t}\rangle - \delta_{\mathrm{P}}(-\mu\overrightarrow{t}), \end{aligned} \tag{6}$$

where

$$\delta_{\mathrm{Box}(\epsilon)}(\overrightarrow{x}) = \begin{cases} 0, & \|\overrightarrow{x}\|_1 \le \epsilon \\ \infty, & \|\overrightarrow{x}\|_1 > \epsilon \end{cases}.$$

Applying the proximal point algorithm to solve (6) and taking an additional extrapolation step, we thus obtain the VEA-DTV algorithm described in **Algorithm 1**, where $\|\cdot\|_2$ is computed by the power method suggested in,[13] $1_J \in \mathbb{R}^J$ denotes the constant vector with all elements set to 1, operator sgn$(\cdot)$ returns the sign of a real number, and $l_1\text{Ball}_a(\cdot)$ projects a vector onto the l_1 ball with radius of a. The symbol neg$(\cdot)$ represents the negative thresholding function, i.e. projects any positive elements of its argument to zero.

Algorithm 1 (VEA-DTV)

Input A, $\overrightarrow{b}, \epsilon, t_y, a$

$L \leftarrow \|K\|_2, K = \left(A^\top, \nu_1\nabla_x^\top, \nu_2\nabla_y^\top, \mu I\right)^\top$, $\sigma \leftarrow \frac{1}{aL}$, $\nu_1 \leftarrow \frac{\|A\|_2}{\|\nabla_x\|_2}$, $\nu_2 \leftarrow \frac{\|A\|_2}{\|\nabla_y\|_2}$, $\mu \leftarrow \frac{\|A\|_2}{\|I\|_2}$

$k \leftarrow 0$

Initialize: $\overrightarrow{u}^{(0)}$, $\overrightarrow{w}^{(0)}$, $\overrightarrow{p}^{(0)}$, $\overrightarrow{q}^{(0)}$ and $\overrightarrow{t}^{(0)}$ to zero

$\overrightarrow{u}^{(0)} \leftarrow \overrightarrow{u}^{(0)}$

repeat

$\overrightarrow{w}'^{(k)} = \overrightarrow{w}^{(k)} + \sigma\left(A\overrightarrow{u}^{(k)} - \overrightarrow{b}\right)$

$\overrightarrow{w}^{(k+1)} = \frac{\overrightarrow{w}'^{(k)}}{\|\overrightarrow{w}'^{(k)}\|_2}\max(\|\overrightarrow{w}'^{(k)}\|_2 - \sigma\epsilon, 0)$

$\overrightarrow{p}'^{(k)} = \overrightarrow{p}^{(k)} + \sigma\nu_1\nabla_x\overrightarrow{u}^k$

$\overrightarrow{p}^{(k+1)} = \frac{\overrightarrow{p}'^{(k)}}{\max(1_I, \overrightarrow{p}'^{(k)})}$

$\overrightarrow{q}'^{(k)} = \overrightarrow{q}^{(k)} + \sigma\nu_2\nabla_y\overrightarrow{u}^k$

$\overrightarrow{q}^{(k+1)} = \overrightarrow{q}'^{(k)} - \sigma\text{sgn}\left(\overrightarrow{q}'^{(k)}\right) l_1\text{Ball}_{\nu_2 t_y}\left(\frac{|\overrightarrow{q}'^{(k)}|}{\sigma}\right)$

$\overrightarrow{t}'^{(k)} = \overrightarrow{t}^{(k)} + \sigma\mu\overrightarrow{u}^k$

$\overrightarrow{t}^{(k+1)} = \text{neg}(\overrightarrow{t}'^{(k)})$

$\overrightarrow{u}^{(k+1)} = \overrightarrow{u}^{(k)} - \tau(A^\top\overrightarrow{w}^{(k+1)} + \nu_1\nabla_x^\top\overrightarrow{p}^{(k+1)} + \nu_2\nabla_y^\top\overrightarrow{q}^{(k+1)} + \mu\overrightarrow{t}^{(k+1)})$

$\overrightarrow{u}^{(k+1)} = 2\overrightarrow{u}^{(k+1)} - \overrightarrow{u}^{(k)}$

$k \leftarrow k + 1$

until stopping criterion is met

Output : $\overrightarrow{u}^{(k)}$

3. EXPERIMENTS

Numerical experiments with simulated data against SART and the DTV algorithm are carried out to validate the effectiveness of the proposed reconstruction algorithm VEA-DTV. The simulated analytic projection data are acquired by the open source software CTSim (http://www.ctsim.org), while the astra toolbox (https://www.astra-toolbox.com/) is utilized to perform the forward and backward projections when they are required.

In terms of parameter selections, since the general CP framwork is adopted, there are totally three parameters subject to tuning, i.e. a, t_y and ϵ for applying VEA-DTV. Correspondingly, there are parameters: a, t_x, t_y, are involved in the DTV algorithm. Ideally, t_x, t_y should be computed in terms of the ideal image. In our experiments, we apply the SART method with 10 iterations on the full-angular data to provide an approximation which then acts like the ideal image. The parameter ϵ relies on noise estimation of the projection data, which might be not easy to acquire. In this work, we tune the parameters to arrive at best performance in terms of artifacts removal and structure-preserving by sampling the parameter space.

3.1 Inverse crime test

The inverse crime occurs when employing the same forward reconstruction model to generate, as well as to invert, synthetic data. To avoid the inverse crime, analytic projection data are acquired in CTSim. Both noise-free and

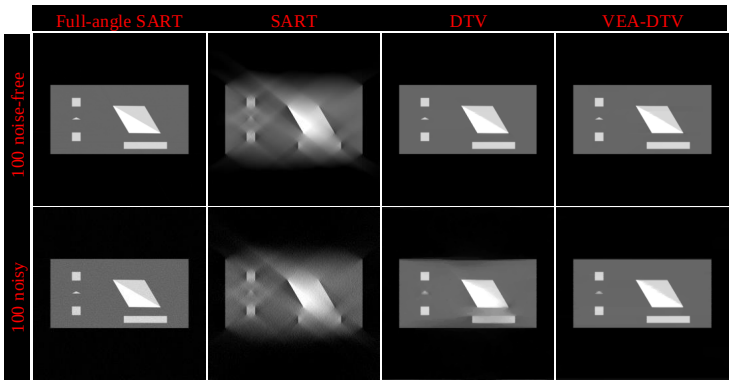

Figure 2: The analytic rectangle phantom. From left to right, the images are reconstructed by full-angle SART, SART, DTV, VEA-DTV, respectively. The first row shows the reconstructions without noise, while the second row shows the results with added Poisson noise, with incidence intensity $I_0 = 1.5 \times 10^5$. The display window is set to [0, 0.5].

noisy projection data are tested. The scanning angular range is set to $[\frac{2\pi}{9}, \frac{7\pi}{9}]$. Poisson noise with incidence intensity $I_0 = 1.5 \times 10^5$ is added to the analytic projection data.

The results are shown in Fig.2. From left to right, the columns 1 and 2 show the SART (10 iterations) reconstructions, with full data and limited data, respectively, and the columns 3 and 4 show the reconstructions of DTV and VEA-DTV, respectively. As Fig.1 has demonstrated, in the limited-angle reconstructions, the invisible edges are too blurred to be recognized. The first row and second row show the noise-free and noisy reconstructions, respectively. We can easily observe that for the noise-free case, DTV and VEA-DTV achieves similar high quality reconstructions, while for the noisy case, VEA-DTV demonstrates superior results. Distortions and blurring could be easily recognized in the DTV reconstructions, especially at the right bottom part. For the proposed VEA-DTV, blurring has been completely removed, and just small local distortions could be identified along the diagonal of the big parallel gram. Same conclusion could be drawn from the quantitative measures listed in Table 1.

Table 1: PSNR, SSIM and NRMSE for the analytic rectangle phantom.

	Index	SART	DTV	VEA-DTV
noise-free	PSNR	22.9650	38.7488	**39.0063**
	SSIM	0.81761	0.99175	**0.99195**
	NRMSE	0.12726	0.00336	**0.00317**
noisy	PSNR	21.8880	31.8155	**34.2304**
	SSIM	0.58396	0.93394	**0.99195**
	NRMSE	0.16308	0.02899	**0.00951**

3.2 Invisible edges recovery capability test

One rhombus phantom with tilt angle of 5 degrees is constructed in CTSim. Its projection data without noise are also acquired in CTSim. Both of them are analytic, which are used to test VEA-DTV's capacity to recover invisible edges. Since the boundary between the two triangles are completely invisible and not distributed along the axes, it is quite challenging to recover it.

The results are shown in Fig.3. From top to bottom, the images are reconstructed with angular ranges 130, 120 and 110 degrees, respectively. From left to right, the columns 2, 3, and 4 show the reconstructions by SART, DTV and VEA-DTV, respectively. As shown in the second column, the SART method fails to recover the invisible edge. For both DTV and VEA-DTV, the quality of the reconstructions decreases with reducing angular ranges, as demonstrated in the last two columns of Fig.3. When the scanning angular range is 130 degrees, both DTV and VEA-DTV recover the invisible edge nearly perfectly. However, when reducing the angular ranges, the

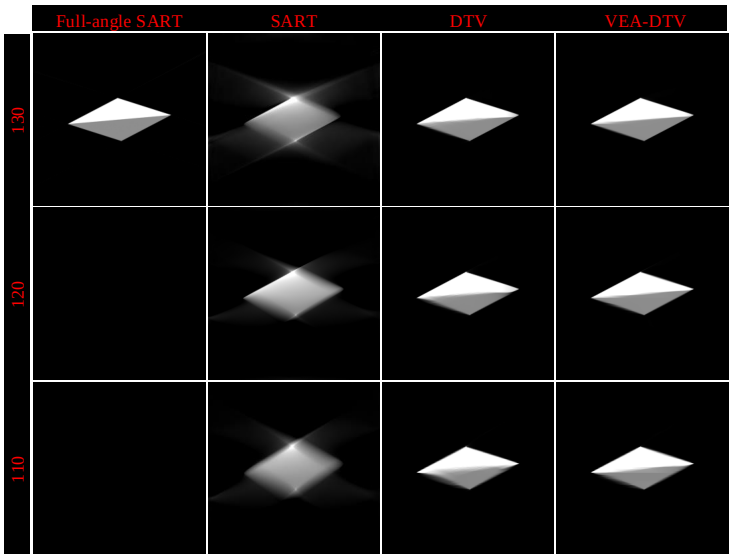

Figure 3: The rhombus phantom. From left to right, the images are reconstruction results from full-angle SART, SART, DTV, STV, respectively. From up to bottom, each row shows the reconstructions with different angular ranges. The display window is set to [0, 0.18].

performance of DTV deteriorates quickly, while the proposed VEA-DTV could demonstrate certain resistances to such changes. Same conclusion could be drawn from the quantitative measures listed in Table 2.

Table 2: PSNR, SSIM and NRMSE for the rhombus phantom.

Angular range	Index	SART	DTV	VEA-DTV
$[\frac{5\pi}{36}, \frac{31\pi}{36}]$	PSNR	24.2663	33.8890	**35.3223**
	SSIM	0.53365	0.99449	**0.99557**
	NRMSE	0.55199	0.01048	**0.00754**
$[\frac{\pi}{6}, \frac{5\pi}{6}]$	PSNR	21.8979	31.8155	**33.7639**
	SSIM	0.89156	0.99177	**0.99376**
	NRMSE	0.16742	0.01690	**0.01079**
$[\frac{7\pi}{36}, \frac{29\pi}{36}]$	PSNR	19.78663	29.9508	**30.5150**
	SSIM	0.85852	0.98734	**0.98829**
	NRMSE	0.27222	0.02597	**0.02279**

4. CONCLUSION

We have proposed a visible edge aware convex model for limited-angle reconstruction which is derived by reformulating a DTV model. By treating the visible edges and the invisible ones differently, the proposed algorithm could make better use of the visible edges prior and achieve better reconstructions. Numerical experiments suggest that, compared to DTV, the proposed VEA-DTV demonstrates improved stability against noise and angular range reducing.

ACKNOWLEDGMENTS

Thanks for the support of the National Natural Science Foundation of China (NSFC) (61971292, 61827809 and 61871275).

REFERENCES

[1] Niklason, L., Christian, B., Niklason, L., Kopans, D., Castleberry, D., Opsahl-Ong, B., Landberg, C., Slanetz, P., Giardino, A., Moore, R., Albagli, D., DeJule, M., Fitzgerald, P., Fobare, D., Giambattista, B., Kwasnick, R., Liu, J., Lubowski, S., Possin, G., and Wirth, R., "Digital tomosynthesis in breast imaging," *Radiology* **205**(2), 399–406 (1997).

[2] Fahrig, R., Dixon, R., Payne, T., Morin, R. L., Ganguly, A., and Strobel, N., "Dose and image quality for a cone-beam C-arm CT system," *Medical Physics* **33**(12), 4541–4550 (2006).

[3] Kudo, H. and Saito, T., "Sinogram recovery with the method of convex projections for limited-data reconstruction in computed tomography," *J. Opt. Soc. Am. A* **8**, 1148–1160 (Jul 1991).

[4] Sidky, E. Y., Kao, C.-M., and Pan, X., "Accurate image reconstruction from few-views and limited-angle data in divergent-beam CT," *Journal of X-ray Science and Technology* **14**(2), 119–139 (2006).

[5] Sidky, E. Y. and Pan, X., "Image reconstruction in circular cone-beam computed tomography by constrained, total-variation minimization," *Physics in Medicine & Biology* **53**(17), 4777 (2008).

[6] Chen, G.-H., Tang, J., and Leng, S., "Prior image constrained compressed sensing (PICCS): a method to accurately reconstruct dynamic CT images from highly undersampled projection data sets," *Medical Physics* **35**(2), 660–663 (2008).

[7] Liu, Y., Ma, J., Fan, Y., and Liang, Z., "Adaptive-weighted total variation minimization for sparse data toward low-dose x-ray computed tomography image reconstruction," *Physics in Medicine & Biology* **57**(23), 7923 (2012).

[8] Quinto, E. T., "Artifacts and visible singularities in limited data X-ray tomography," *Sensing and Imaging* **18**(1), 9 (2017).

[9] Chen, Z., Jin, X., Li, L., and Wang, G., "A limited-angle CT reconstruction method based on anisotropic TV minimization," *Physics in Medicine & Biology* **58**(7), 2119 (2013).

[10] Wang, T., Nakamoto, K., Zhang, H., and Liu, H., "Reweighted anisotropic total variation minimization for limited-angle CT reconstruction," *IEEE Transactions on Nuclear Science* **64**(10), 2742–2760 (2017).

[11] Xu, J., Zhao, Y., Li, H., and Zhang, P., "An image reconstruction model regularized by edge-preserving diffusion and smoothing for limited-angle computed tomography," *Inverse Problems* **35**(8), 085004 (2019).

[12] Zhang, Z., Chen, B., Xia, D., Sidky, E. Y., and Pan, X., "Directional-tv algorithm for image reconstruction from limited-angular-range data," *Medical Image Analysis* **70**, 102030 (2021).

[13] Sidky, E. Y., Jørgensen, J. H., and Pan, X., "Convex optimization problem prototyping for image reconstruction in computed tomography with the chambolle–pock algorithm," *Physics in Medicine and Biology* **57**, 3065–3091 (apr 2012).

[14] Bertsekas, D. P. et al., "Incremental gradient, subgradient, and proximal methods for convex optimization: A survey," *Optimization for Machine Learning* **2010**(1-38), 3 (2011).